LASER PLASMA

PACS numbers: 32.50.+d, 32.70.Jz, 52.25.Os
DOI: 10.1070/QE2009v039n12ABEH014094

Resonant optical characteristics of an ultracold laser plasma

N.I. Kosarev, N.Ya. Shaparev

***Abstract*. We report a computer simulation study of light absorption, scattering and emission at 397 nm in an ultracold calcium ion plasma under resonant excitation. The results point to spectral asymmetry of light scattering, nonlinear absorption, and emission in the plasma. An approach is proposed for ultracold plasma diagnostics using resonant optical characteristics.**

Keywords: *ultracold laser plasma, resonant excitation, optical characteristics.*

1. Introduction

Gavriluk et al. [1 – 3] proposed the concept of cooling an electron-ion plasma by resonant laser radiation and confining the ions in a magneto-optical trap. Later, this approach was used in simulations of the cooling of expanding photoionised plasmas [4]. Ultracold plasmas have attracted considerable interest owing to the first experimental studies [5 – 7] in which laser-cooled Xe atoms were photoionised to produce an ultracold plasma with ion and electron temperatures $T_i \approx 1$ K and $T_e \approx 1000$ K, respectively, and a density of charged particles $n \approx 10^6 - 10^9$ cm^{-3}. To probe ultracold plasmas at small optical depths, Simien et al. [8] used resonant absorption imaging.

In this paper, we report a computer simulation study of light scattering, absorption and emission in an expanding ultracold calcium plasma on the $^2S_{1/2} \leftrightarrow {}^2P_{1/2}$ transition ($\lambda = 397$ nm) at different optical depths.

2. Plasma model

Photoionisation of cooled atoms is followed by plasma expansion in vacuum as represented by [9]

$$\sigma(t) = (\sigma_0^2 + v_e^2 t^2)^{1/2}, \tag{1}$$

where $\sigma(t)$ is the rms radius of the Gaussian ion distribution; σ_0 is the initial radius of the distribution; v_e is the electron thermal velocity; and t is time. The ion density $N_0(r,t)$, ion temperature $T_i(r)$, and radial ion velocity $\boldsymbol{v}(r,t)$ distributions can be represented in the form [4 – 8]

$$N_0(r,t) = n_0[\sigma_0^3/\sigma^3(t)]\exp(-r^2/\sigma^2(t)), \tag{2}$$

$$T_i(r,t) = T_0\exp(-r^2/3\sigma^2(t)), \tag{3}$$

$$\boldsymbol{v}(r,t) = \frac{v_e^2 t\,\boldsymbol{r}}{\sigma^2(t)}, \tag{4}$$

where n_0 and T_0 are the ion density and ion temperature in the centre of the cloud at time zero, and r is a variable coordinate. The factor $\sigma_0^3/\sigma^3(t)$ on the right-hand side of (2) is due to the normalisation of the ion density $N_0(r,t)$ to the total number of particles in the plasma at time zero.

The radial expansion of the plasma contributes to the Doppler broadening of the spectrum. The line shape is then given by [10]

$$\Phi(x-\mu V,r,t) = \pi^{-1/2}[\delta(r)]^{-1} \times \exp\{-(x-\mu V)^2/[\delta(r)]^2\}. \tag{5}$$

Here, $x = (\nu - \nu_0)/\Delta\nu_D^*$ is the difference between frequency ν and the centre frequency ν_0 in units of the Doppler width, $\Delta\nu_D^*$, which is related to the ion thermal velocity in the centre of the spherical cloud, v_i^*, by $\Delta\nu_D^* = \nu_0 v_i^*/c$; c is the speed of light; $\mu = \cos\theta$; θ is the angle between the ion velocity and the direction to the observer; $V = v(r,t)/v_i$; v_i is the ion thermal velocity at point r; $\delta(r) = \Delta\nu(r,t)/\Delta\nu_D^*$ is the linewidth in units of $\Delta\nu_D^*$; and $\Delta\nu(r,t)$ is the full width of the Doppler profile at point r, which depends on the temperature and the macroscopic velocity of the plasma at this point at time t. The broadening due to the macroscopic plasma expansion, $\delta\nu$, at point r and time t is $\delta\nu(r,t) = \nu_0 v(r,t)/c = v(r,t)/\lambda$, where λ is the wavelength of the transition. Therefore, the absorption linewidth is given by

$$\Delta\nu(r,t) = \Delta\nu_D(r) + \frac{|v(r,t)|}{\lambda}, \tag{6}$$

where $\Delta\nu_D$ is the Doppler width at an arbitrary point of the plasma.

The kinetics of ion excitation are described by the rate equations for the radiation-controlled population balance

N.I. Kosarev, N.Ya. Shaparev Institute of Computational Modeling, Siberian Branch, Russian Academy of Sciences, Akademgorodok, 660036 Krasnoyarsk, Russia;
e-mail: kosarev_nikolai@mail.ru, shaparev@icm.krasn.ru

Received 2 March 2009; revision received 24 September 2009
Kvantovaya Elektronika **39** (12) 1112 – 1116 (2009)
Translated by O.M. Tsarev

$$\frac{dN_1(r,t)}{dt} = -B_{12}JN_1(r,t) + (B_{21}J + A_{21})N_2(r,t), \quad (7)$$

$$\frac{dN_2(r,t)}{dt} = -(B_{21}J + A_{21})N_2(r,t) + B_{12}JN_1(r,t), \quad (8)$$

and the equation of conservation of the number of particles

$$N_1(r,t) + N_2(r,t) = N_0(r,t) \quad (9)$$

with the initial conditions at time $t = 0$

$$N_1(r,0) = N_0(r),\ N_2(r) = 0,$$

where N_1 and N_2 are the ion ground and excited state populations, and A_{21}, B_{12} and B_{21} are the Einstein coefficients for the spontaneous decay, stimulated radiative excitation, and quenching probabilities. In Eqns (7) and (8), $J(r,t)$ is the angle/frequency averaged light intensity at point r and time t, due to the laser radiation and scattering:

$$J(r,t) = \frac{1}{4\pi}\int_0^{2\pi} d\phi \int_0^{\pi} \sin\vartheta d\vartheta \times \int_{-\infty}^{\infty} \Phi(x - \mu V)\, I(r,\vartheta,\phi,x,t)dx. \quad (10)$$

The light intensity, $I(r,\vartheta,\phi,v,t)$, was determined in a quasi-steady-state approximation by solving the transfer equation

$$\frac{dI}{d\tau} = \Phi(x-\mu V)(S - I), \quad (11)$$

with the following boundary condition for the radiation incident on a sphere of radius R:

$$I(R,\vartheta,\phi,v) = \begin{cases} 0, & \text{for } \vartheta \neq 0, \\ I_{las}(v,t), & \text{for } \vartheta = 0. \end{cases} \quad (12)$$

Here, $d\tau = \kappa_0(r)dr$;

$$\kappa_0(r) = \frac{c^2 A_{21} g_2}{8\pi v_0^2 g_1}\left(N_1 - \frac{g_1}{g_2}N_2\right)$$

is the absorption coefficient at the centre frequency;

$$S(r) = \frac{2hv_0^3 g_1}{c^2 g_2}\frac{N_2}{N_1 - (g_1/g_2)N_2} \quad (13)$$

is the source function, which takes into account the absorbed laser radiation and scattered radiation; $\hbar$ is the Planck constant; and g_1 and g_2 are the statistical weights of states 1 and 2. The excitation laser pulse, $I_{las}(v,t)$, had a homogeneous transverse profile with a cross-sectional size exceeding the diameter of the cloud.

3. Numerical simulation results

The system of integro-differential equations (7)–(13) with the plasma parameters in the form (1)–(6) was solved numerically using an approach described elsewhere [11] and applied in recent studies [12, 13]. In the computations, we used the following model parameters at $t = 0$: calcium ion temperature in the centre of the spherical cloud $T_0 = 1$ K, rms radius of the Gaussian ion distribution $\sigma_0 = 0.02$ cm, and radius of the spherical cloud $R_0 = 0.05$ cm. The optical depth at the centre frequency of the spectral profile was determined along a diameter of a spherical droplet, $\tau_0 = \int_{-\infty}^{\infty}\kappa_0(r)dr$, at time zero. The plasma expansion velocity, v, was specified at point σ_0. The absorption line profile took into account the combined effect of the Lorentzian and Doppler broadening mechanisms using a Voigt profile. The Lorentzian width accounted for the radiative ($\Delta\nu_{rad} = A_{21}/2\pi$) and collisional ($\Delta\nu_{col} = 0.4 \times 10^{-7} N_0$) broadening mechanisms. The simulation results below correspond to observation along a diameter of the spherical cloud.

3.1 Laser radiation absorption

Figure 1 shows the relative intensity of the transmitted broadband radiation at different plasma expansion velocities. The radial expansion of the ion cloud reduces the absorption at the centre frequency and increases that in the wings. As a result, the transmitted intensity increases around the centre frequency and decreases in the wings. The effect, of course, becomes stronger with increasing expansion velocity.

At large optical depths, the spectral distribution of the transmitted light depends on the incident intensity. Figure 2 shows the spectral distributions of the relative laser light intensity at different points of the medium. At the beginning of the path and up to the centre of the sphere [Fig. 2a, curves (*1–3*)], the ions and photons move in opposite directions. Because of this, the absorption band is red-shifted, and the laser light is more strongly absorbed at longer wavelengths than at shorter wavelengths (in the blue). After the centre of the sphere is passed, the light is absorbed by the ions that move in the same direction as the photons. As a result, the absorption is stronger at shorter wavelengths, and the light emerging from the plasma has a symmetrical spectrum [Fig. 2a, curve (*6*)].

At high intensities, the absorption is nonlinear [Fig. 2b, curves (*1–6*)]. At the beginning of the path and up to the centre of the sphere, the red wing of the line is absorbed by the plasma layer that moves in the opposite direction. At the

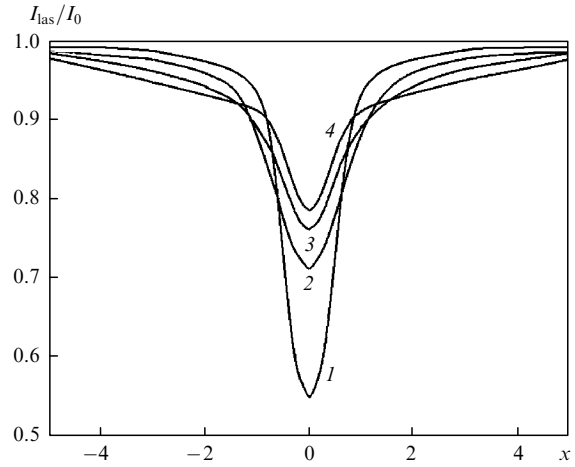

Figure 1. Bleaching caused by plasma expansion at $v = 0$ (*1*), 2×10^3 (*2*), 4×10^3 (*3*) and 6×10^3 cm s^{-1} (*4*); $I_0 = 10^{-13}$ W cm^{-2} Hz^{-1}, $\tau_0 = 1$.

same time, the distant absorption wings in this region of the medium lead to absorption, though weaker, in the blue wing. Since the light intensity is highest when the pulse enters the plasma, the nonlinear effect here is very significant. After the centre of the sphere is passed, the absorption is stronger in the blue spectral region, but this region, with an already reduced intensity, causes a weaker nonlinear absorption, and the absorption here shows nearly linear behaviour. As a result, the transmitted radiation has an asymmetric spectrum [Fig. 2b, curve (*6*)]. Qualitatively similar behaviour was observed in the case of narrow-band laser radiation [13].

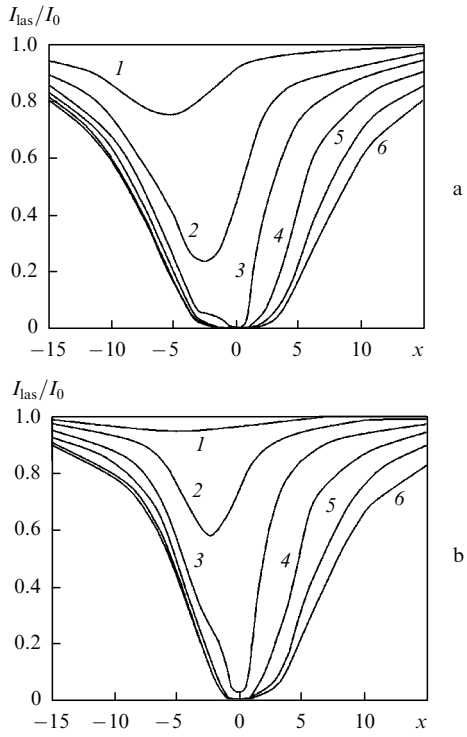

Figure 2. (a) Linear ($I_0 = 10^{-13}$ W cm^{-2} Hz^{-1}) and (b) nonlinear ($I_0 = 10^{-8}$ W cm^{-2} Hz^{-1}) resonant absorption in an expanding plasma at $r = -0.025$ (*1*), -0.013 (*2*), 0 (centre of the sphere) (*3*), 0.013 (*4*), 0.025 (*5*) and 0.05 cm (emerging radiation) (*6*); $\tau_0 = 20$, $v = 6 \times 10^3$ cm s^{-1}.

3.2 Laser radiation scattering

As mentioned above, laser radiation incident on a sphere and then propagating into it has the greatest absorption coefficient in its red wing. Spontaneous emission in the light propagation direction (forward scattering) has the same frequency as the absorbed light and is more weakly absorbed along its entire path across the sphere. Spontaneous emission in the opposite direction (backscattering) lies in the blue spectral region. The blue wing of the laser radiation is also absorbed before the centre of the sphere, though more weakly than the red wing. Spontaneous emission from the sphere in the forward direction contributes to the red wing of the scattered light, and that in the opposite direction (backward) remains blue. After the centre of the sphere, the blue wing of the laser radiation is absorbed more strongly. Spontaneous emission from the sphere in the forward direction retains its frequency, and that in the backward direction lies in the red spectral region. Because the blue wing of the laser light already has a low intensity in this region, it cannot compensate the asymmetry of the backscatter spectrum in the blue.

Thus, the backscattered light is blue-shifted, and the forward-scattered one is red-shifted. Multiple scattering enhances this process, as evidenced by the simulation results presented in Fig. 3. It follows from the shape of curve (*3*) that the scattering spectrum becomes almost symmetrical, which is due to the competition between the forward scattering and backscattering processes. Note that the blue and red shifts increase with expansion velocity.

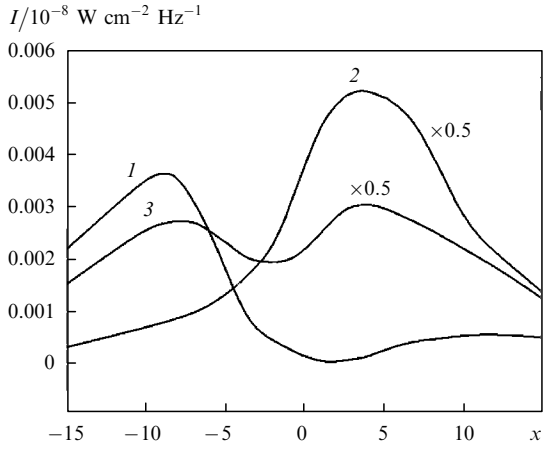

Figure 3. Scattered-light spectra: forward scattering (*1*), backscattering (*2*), 75° scattering (*3*); $I_0 = 10^{-8}$ W cm^{-2} Hz^{-1}, $\tau_0 = 50$, $v = 6 \times 10^3$ cm s^{-1}.

3.3 Afterglow emission from an ultracold plasma

Optical emission from the plasma was simulated as radiative decay of ions excited to saturation. In the initial conditions ($t = 0$) for Eqns (7) and (8), the populations were taken to be $N_2 \approx 0.5N_0$, $N_1 \approx 0.5N_0$.

The light propagating outwards from the spherical cloud is absorbed by the ions mainly in the blue spectral region. The red light arriving at the boundary of the cloud from its interior is more weakly absorbed. Because of this, the emerging afterglow emission is red-shifted, and the red shift of the scattered-light spectrum increases as the excited state decays. Figure 4 illustrates the time variation of the emission spectrum of the plasma.

3.4 Expansion velocity of an optically thin plasma

The plasma expansion velocity v at $r = \sigma_0$ as a function of average thickness $\Delta\bar{\nu}$ was determined numerically using the formula

$$\Delta\bar{\nu} = \int_{-\infty}^{\infty} N_0 \Delta\nu \mathrm{d}r \Big/ \int_{-\infty}^{\infty} N_0 \mathrm{d}r$$

$$\approx \int_{-\infty}^{\infty} n_0 \exp(-r^2/\sigma^2)\Delta\nu \mathrm{d}r \Big/ \int_{-\infty}^{\infty} n_0 \exp(-r^2/\sigma^2)\mathrm{d}r. \quad (14)$$

The results can be approximated by

$$v = 4 \times 10^{-5} \Delta\nu, \quad (15)$$

where v is in centimetres per second and $\Delta\nu$ is in hertz.

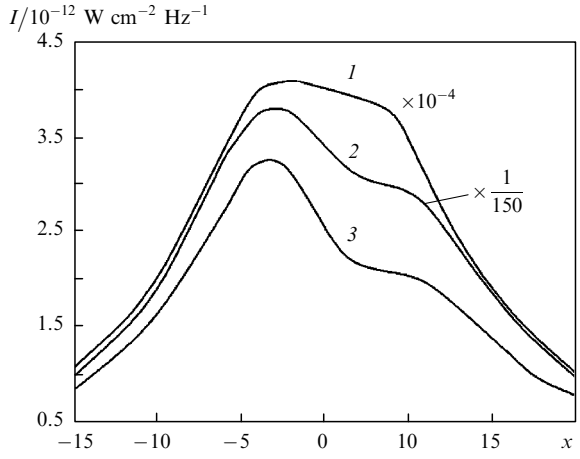

Figure 4. Emission spectra of the plasma at $t = 10$ (*1*), 50 (*2*) and 100 ns (*3*); $\tau_0 = 50$, $v = 6 \times 10^3$ cm s^{-1}.

3.5 Normal-ion density at low expansion velocities in an optically dense medium

To evaluate the normal-ion density in the plasma, we find the frequency at which the absorption in the plasma reduces the light intensity by a factor of 10. We refer to this frequency as the cutoff frequency and denote it in units of the Doppler width as x_c. At this frequency, the exponent in Bouguer's law must be 2.3. Assume that the plasma is at rest at time zero. Then, using the Doppler line shape (5) with $V = 0$, we obtain the following relation for x_c:

$$\int_{-\infty}^{\infty} \frac{\kappa_0 e^{-x_c^2}}{\sqrt{\pi}} dl = 2.3. \tag{16}$$

Substituting (1) and κ_0 from (13) into (16) and integrating, we obtain for time $t = 0$

$$n_0 = \frac{2.3}{\sigma_{abs}\sigma_0} e^{x_c^2}, \quad \sigma_{abs} = \frac{c^2 A_{21}}{8\pi\nu_0^2}\frac{g_2}{g_1}\frac{1}{\Delta\nu_D}. \tag{17}$$

The plot of n_0 against x_c with the above parameters of the calcium ion is presented in Fig. 5.

3.6 Expansion velocity of an optically dense plasma

In the initial stages of plasma formation, the expansion velocity of the ion cloud is close to zero, so the ion density can be evaluated from the cutoff frequency. In later stages, when the expansion velocity of the ultracold plasma cannot be neglected, Eqn (16) takes the form

$$\int_{-\infty}^{\infty} \frac{\kappa_0 e^{-(x_c-\mu V)^2\delta^{-2}}}{\sqrt{\pi}} dl = 2.3. \tag{18}$$

To calculate the integral in (18), we take into account that, in a given observation direction, the plasma has the form of two flat layers moving in opposite directions relative to the centre of the sphere. The left-hand side of Eqn (18) can then be represented as two terms,

$$\frac{1}{\sqrt{\pi}}\int_{-\infty}^{0} \sigma_{abs} n_0 \exp(-r^2/\sigma_0) \exp\left\{-\left[x_c + \frac{v(r)}{v^*}\right]^2 \times \left[\frac{\Delta\nu_D^*}{\Delta\nu_D^* + v(r)/\lambda}\right]^2\right\} dr + \frac{1}{\sqrt{\pi}}\int_0^{\infty} \sigma_{abs} n_0 \exp(-r^2/\sigma_0) \times \exp\left\{-\left[x_c - \frac{v(r)}{v^*}\right]^2 \left[\frac{\Delta\nu_D^*}{\Delta\nu_D^* + v(r)/\lambda}\right]^2\right\} dr = 2.3, \tag{19}$$

where the thermal Doppler width $\Delta\nu_D^*$ can be expressed through the thermal velocity and the wavelength of the transition: $\Delta\nu_D^* = v/\lambda$.

The ion density n_0 in Eqn (19) can be determined from the cutoff frequency of the plasma at rest (see Fig. 5). Then, (19) is a transcendental equation which can be solved numerically to obtain the expansion velocity as a function of x_c. To this end, the integrals in (19) were replaced by quadrature sums corresponding to the trapezium method. Figure 6 plots the relative expansion velocity v/v^* against x_c at different n_0 values determined from Fig. 5. The shape of the curves in Fig. 6 indicates that, in an optically dense plasma, the cutoff frequency increases with expansion velocity, i.e., macroscopic expansion of the ion cloud leads to broadening of the absorption line and an increase in cutoff frequency.

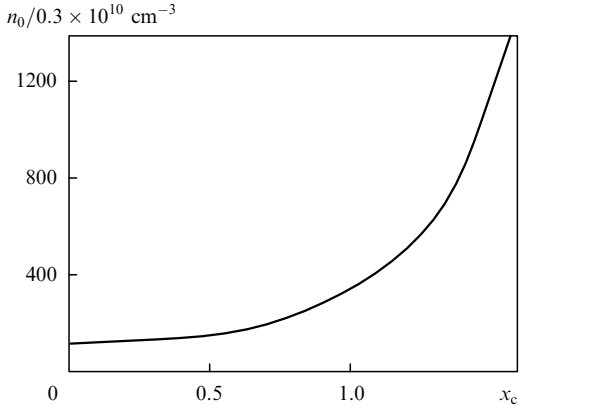

Figure 5. Calcium ion density n_0 as a function of cutoff frequency x_c for a stationary medium.

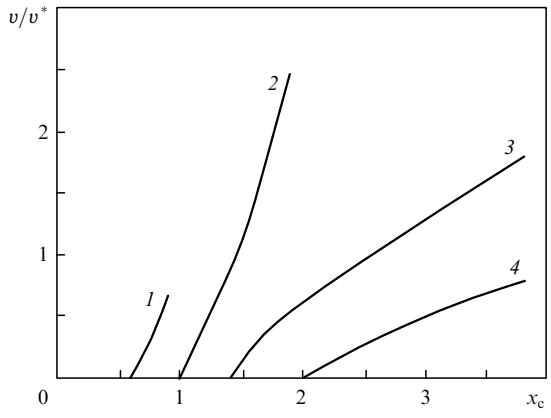

Figure 6. Relative expansion velocity v/v^* as a function of cutoff frequency x_c at ion densities $n_0 = 5.4 \times 10^{11}$ (*1*), 10^{12} (*2*), 2.7×10^{12} (*3*), 2×10^{13} (*4*) cm^{-3}.

4. Conclusions

We considered light absorption, scattering and emission in an expanding ultracold plasma. Mathematically, the problem was formulated in terms of a system of integro-

differential equations, which was solved numerically using a specialised algorithm.

The results point to spectral asymmetry of nonlinear absorption in the plasma, a blue shift of the backscattered light, red shift of the forward-scattered light and red shift of the emission spectrum.

We proposed approaches for determining the ion density and velocity in optically dense plasmas by measuring the light intensity in the wings of the absorption line.

The expansion of the ion cloud is predicted to cause bleaching at the centre frequency (increased absorption in the wings).

References

1. Gavriluk A.P., Krasnov I.V., Shaparev N.Ya. *Pis'ma Zh. Eksp. Teor. Fiz.*, **63**, 316 (1996).
2. Gavriluk A.P., Krasnov I.V., Shaparev N.Ya. *Pis'ma Zh. Tekh. Fiz.*, **23**, 28 (1997).
3. Gavriluk A.P., Krasnov I.V., Shaparev N.Ya. *Laser Phys.*, **8**, 653 (1998).
4. Pohl T., Pattard T., Rost J.M. *Phys. Rev. Lett.*, **92** (15), 155003-1 (2004).
5. Killian T.C., Kulin S., Bergeson S.D., et al. *Phys. Rev. Lett.*, **83** (23), 4776 (1999).
6. Kulin S., Killian T.C., Bergeson S.D., et al. *Phys. Rev. Lett.*, **85** (2), 318 (2000).
7. Killian T.C., Lim M.J., Kulin S., et al. *Phys. Rev. Lett.*, **86** (17), 3759 (2001).
8. Simien C.E., Chen Y.C., Gupta P., et al. *Phys. Rev. Lett.*, **92**, 143001-1 (2004).
9. Dorozhkina D.S., Semenov V.E. *Pis'ma Zh. Eksp. Teor. Fiz.*, **67** (8), 543 (1998).
10. Mihalas D. *Stellar Atmospheres* (San Francisco: Freeman, 1978; Moscow: Mir, 1982) Vol. 2.
11. Kosarev N.I. *Mat. Model.*, **18** (12), 67 (2006).
12. Kosarev N.I., Shaparev N.Ya. *Dokl. Akad. Nauk*, **421** (6), 762 (2008).
13. Kosarev N.I., Shaparev N.Ya. *J. Phys. B: At. Mol. Opt. Phys.*, **41**, 235701-1 (2008).